Pulsed Excitation of a Single Atom

Sandoko Kosen

an academic exercise presented in partial fulfillment for the degree of Bachelor of Science with Honours in Physics

Supervisor: Professor Christian Kurtsiefer

Department of Physics

National University of Singapore

2014

Abstract

Interfacing different physical systems is important in the context of building a practical quantum information network. As a first step towards interfacing different physical systems, we aim to demonstrate the indistinguishability between single photons produced via two different processes by observing the Hong-Ou-Mandel interference effect. The single photons are produced via a four-wave mixing process in a cold atomic ensemble of ^{87}Rb and spontaneous emission from a single ^{87}Rb atom in an optical dipole trap. This thesis reports the progress of the single ^{87}Rb atom setup towards achieving this goal. We measure the temporal profile of the spontaneously emitted single photon and show that the characteristic decay time is in accordance with the values in the literature. Finally, we demonstrate that we can excite the atom with an excitation probability of 78% using a π pulse.

Acknowledgements

I would like to thank Professor Christian Kurtsiefer for the opportunity to work in this single atom project. It has been a real pleasure working in his lab. Prior to joining his group, my idea of experimental physics is all about simple setup and taking data. Now that I have worked in the single atom setup for almost eight months, I realise the other aspects of experimental physics like electronics, programming, etc. that are essential in building and maintaining complex setup.

The second person I would like to thank is Victor that has been working with me in this project. He taught me many things: from electronics to physics. He also went through the pain of reading the very first draft of this thesis and being critical to whatever I wrote in this thesis.

To Gleb, he was always there to answer whatever stupid questions I had in mind (and at the same time not making me feel like one). I thank him for all the encouragement and the knowledge. I wish him all the very best in his future career.

I would also like to thank everyone else in the lab, especially Wilson and Chi Huan for making my daily life in lab more enjoyable. Arifin, Chern Hui and Raymond for being very good friends since we met.

Lastly, I would like to thank my family for always being there and supporting me in doing physics. They have always cared for me. No word can express my gratitude to them.

Contents

1

Introduction

1.1 Towards Interfacing Two Different Systems

In the past two decades, research in quantum information has given rise to new fields, such as quantum communication [1] and quantum computation [2], that can perform tasks beyond what is possible using conventional technology. To realize this, one can imagine a quantum network [3] that consists of multiple quantum nodes interconnected by quantum channels. In each quantum node, the quantum information is produced, processed and stored while it is reliably transferred between the nodes and eventually across the network through the quantum channels.

Different physical systems have been proposed as the candidates for the implementation of a quantum network. Examples are trapped ions [4], trapped atoms [5, 6], nitrogen-vacancy centers [7], etc. Each has its own features that make it suited only for a particular quantum information processing protocol. In an effort to realize a large scale quantum network, it is therefore important to be able to interface different physical systems.

Our research group has developed two different systems in the lab. The first system is a single ^{87}Rb atom trapped in an optical dipole trap that is able to emit a single photon through a spontaneous emission process [8]. The second system is an atomic ensemble of ^{87}Rb that produces entangled photon pairs via a

four-wave mixing process [9]. The detection of one photon of the entangled pair will herald the existence of the other single photon of the entangled pair.

The two systems can be regarded as two different nodes in the context of a quantum network. As a first step towards interfacing the two different systems, we want to demonstrate the indistinguishability between the two photons emitted by the two different physical systems. This can be done by performing an experiment similar to the Hong-Ou-Mandel two-photon interference experiment [10]. In that experiment, they showed that two indistinguishable photons impinging on a 50/50 beam splitter will emerge together from either of the output ports of the beam splitter. Consequently, one should observe a zero coincidence count between the two detectors at the output ports of the beam splitter.

This thesis reports on the progress towards demonstrating the indistinguishability between the two single photons emitted by the two different systems. My work focuses on the single atom system. The goal is to use the single atom as a single photon emitter by sending an optical pulse to excite the single atom along a closed two-level cycling transition. By tuning the parameters of the optical pulse, the atom can be made to emit a single photon with the highest probability.

The organization of the thesis is as follows: we first present the measurement of the resonance frequency of the two-level cycling transition used to generate a single photon. Then it continues with a pulsed excitation experiment where we sent a short optical pulse to the single atom and measured the excitation probability of the optical pulse. The strategy is to fix the duration of the optical pulse and vary the amplitude of the optical pulse such that we achieve the highest excitation probability. Finally, we conclude and briefly discuss the future setup for the joint experiment.

1.2 Basics of the Single Atom Setup

We choose to work with ^{87}Rb because it possesses closed two-level cycling transitions. To describe the fine structure of ^{87}Rb, we use the following notation: nL_J where n denotes the principal quantum number, L denotes the total orbital angular momentum quantum number and J denotes the total electron angular

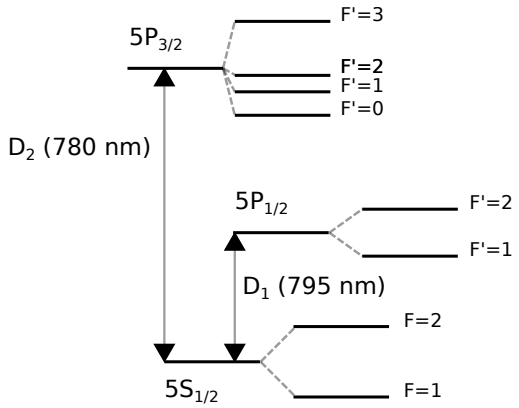

Figure 1.1: Energy level diagram of ^{87}Rb showing the $5S_{1/2}$ ground state, the $5P_{1/2}$ and $5P_{3/2}$ excited states and their corresponding hyperfine sublevels. Diagram not drawn to scale.

momentum quantum number. Two important transition lines relevant to this work are (Fig. 1.1): $5S_{1/2} \rightarrow 5P_{1/2}$ (D_1 line, $\approx 795\,\text{nm}$) and $5S_{1/2} \rightarrow 5P_{3/2}$ (D_2 line, $\approx 780\,\text{nm}$). To describe the hyperfine interaction between the electron and the nuclear angular momentum I, we denote $F = J + I$ as the total atomic angular momentum.

In our setup, we achieve substantial atom-light interaction in free space [8] by strongly focusing the probe laser beam to a diffraction-limited spot size as illustrated in Fig. 1.2. The basic setup consists of two confocal aspheric lenses with effective focal length of 4.5 mm (at 780 nm) enclosed in an ultra high vacuum chamber. The lenses are designed to transform a collimated laser beam into a diffraction-limited spot size at the focus of the lens with minimal spherical aberration.

To trap a single atom, we start with an atomic cloud in a magneto-optical trap (MOT) and use an optical dipole trap to trap a single atom at the focus of the lens[1].

A MOT consists of three pairs of counter-propagating laser beams that intersect at the center of a quadrupole magnetic field. The quadrupole field is created by a pair of anti-Helmholtz coils, while three other orthogonal pairs of Helmholtz coils are used to compensate for stray magnetic fields (coils not shown in Fig. 1.2).

[1]For complete details on the operation of a MOT and optical dipole trap, refer to [11]

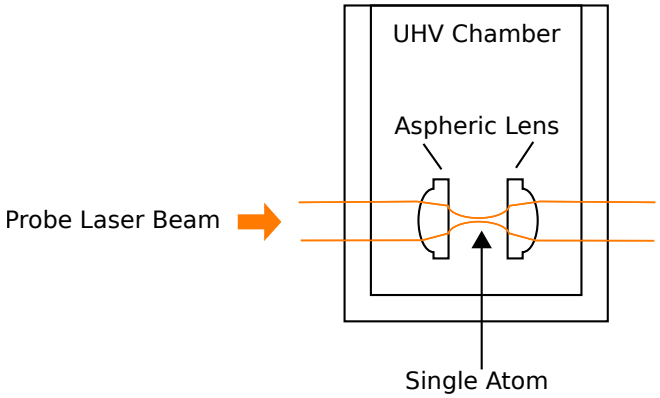

Figure 1.2: Strong atom-light interaction achieved through strong focusing.

The MOT is used to slow down the atoms and at the same time compress them toward the centre of the quadrupole magnetic field.

Each MOT laser beam consists of a cooling beam red detuned (to compensate for the Doppler shift) from the $|5S_{1/2}, F = 2\rangle \rightarrow |5P_{3/2}, F' = 3\rangle$ transition and a repump beam tuned to the $|5S_{1/2}, F = 1\rangle \rightarrow |5P_{1/2}, F' = 2\rangle$ transition. The MOT cooling beam cools the atomic cloud. Off-resonant excitation induced by the MOT cooling beam may cause the atom to decay to the $|5S_{1/2}, F = 1\rangle$ of ground state. The MOT repump beam empties the $|5S_{1/2}, F = 1\rangle$ state by exciting it to $|5P_{1/2}, F' = 2\rangle$, from which the atoms can decay back to the $|5S_{1/2}, F = 2\rangle$ of ground state and continue to participate again in the cooling process.

The optical dipole trap is a far-off-resonant trap (FORT) that consists of a red detuned Gaussian laser beam at 980 nm (far detuned from the optical transitions of ^{87}Rb) that is focused by the aspheric lens (the same lens that focuses the probe beam). Therefore a large intensity gradient is created at the focus of the lens. As the dipole trap is red-detuned, the atom will be attracted towards the region with the highest intensity at the focus of the lens.

The optical dipole trap operates in the collisional blockade regime [12, 13]. As soon as there are two particles in the trap, the collision between the particles in the trap will become the dominant loss mechanism and kick both atoms out of trap. As such, there can either be only 0 or 1 atom in the trap. The presence of a single atom in the trap can be seen from the detection signal that jumps between two discrete levels. When there is no atom in the trap, the detector detects the

background noise. With one atom in the trap, the detector detects a higher discrete level which is the atomic fluorescence. The presence of a single atom has also been independently verified by the measurement of the second-order autocorrelation function of the atomic fluorescence between two independent detectors ($g^{(2)}(\tau)$, where τ is the time delay between the two detectors). The value of the second-order autocorrelation function has been shown to drop below 0.5 at $\tau = 0$, which is the signature of a single emitter [8].

2

Measurement of the Resonance Frequency

2.1 Introduction

The energy levels of the trapped atom are shifted due to the AC-Stark shift induced by the presence of the dipole trap beam. It is therefore important to measure the resonance frequency of this optical transition in order to excite the atom with a high excitation probability.

To do this, we send probe beam to the atom (Fig. 1.2) and measure the transmitted power as a function of its optical frequency. We should observe the largest decrease in the transmission when the optical frequency matches the resonance frequency of the optical transition. In the following, we refer to this experiment as the transmission experiment.

This experiment is similar to that performed by Tey, MK et al [8] in 2008. Whereas the objective of Tey's experiment was to show that it is possible to achieve substantial atom-light interaction through strong focusing in free space, here we are more interested in the resonance frequency of the optical transition we are exciting.

The organization of this chapter is as follows: we first present the optical transition of the atom that we are exciting. Next, we proceed to present the

experimental setup and the experimental sequence for the transmission experiment. Finally, we show that by repeating the experimental sequence for different frequency of probe beam, we observe a change in the transmission. The largest decrease in the transmission indicates that the probe beam is on resonance with the optical transition.

2.2 Effective Two-Level System in ^{87}Rb

Fig. 2.1 shows the $|5S_{1/2}, F = 2, m_F = \pm 2\rangle \rightarrow |5P_{3/2}, F' = 3, m_{F'} = \pm 3\rangle$ transition in ^{87}Rb atom (D_2 line). Each of these transitions forms a closed cycling transition and can only be excited by probe beam circularly polarized with the correct handedness with respect to the quantization axis of the atom. Therefore, exciting ^{87}Rb atom along one of these transitions allows us to approximate a multi-level ^{87}Rb atom as an effective two-level system.

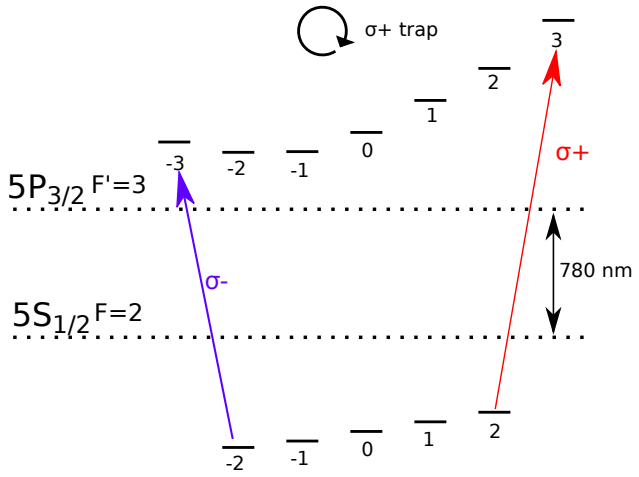

Figure 2.1: Energy level diagram of a single ^{87}Rb atom trapped in a far-off-resonance dipole trap showing the $F = 2$ to $F' = 3$ levels of the D_2 transition with their m_F sublevels. The different positions of the m_F sublevels are shifted by the AC Stark effect induced by the presence of σ_+ polarized dipole trap.

To illustrate the closed cycling transition, consider an atom initially prepared in $|5S_{1/2}, F = 2, m_F = +2\rangle$. Then a σ_+ beam (right circularly polarized with respect to the quantization axis of the atom) on resonance will excite the atom only to $|5P_{3/2}, F' = 3, m_{F'} = +3\rangle$. The nearest $m_{F'}$ sublevels of the excited

state remain untouched because conservation of total angular momentum only allows $\Delta m_F = +1$ transition and $m_{F'} = +3$ can only be found in $|5P_{3/2}, F' = 3\rangle$. The decay process allows $\Delta F = 0, \pm 1$ and $\Delta m_F = 0, \pm 1$. This leaves $|5S_{1/2}, F = 2, m_F = +2\rangle$ as the only possible final state after the decay. Thus an atom excited to $|5P_{3/2}, F' = 3, m_{F'} = +3\rangle$ can only decay to $|5S_{1/2}, F = 2, m_F = +2\rangle$. In this way, the $|5S_{1/2}, F = 2, m_F = +2\rangle$ to $|5P_{3/2}, F' = 3, m_{F'} = +3\rangle$ transition is a closed cycling transition. Similarly, the $|5S_{1/2}, F = 2, m_F = -2\rangle \rightarrow |5P_{3/2}, F' = 3, m_{F'} = -3\rangle$ transition is a closed cycling transition and can only be probed by a σ_- beam. In this experiment, we choose to excite the latter transition.

In practice, the polarization of the probe beam always contains a small amount of other polarization that may cause an off-resonant excitation to other hyperfine levels of the excited state. This may cause the atom to subsequently decay to the $|5S_{1/2}, F = 1\rangle$ ground state and exit the closed cycling transition. To correct for this, we added another repump beam that is tuned to $|5S_{1/2}, F = 1\rangle \rightarrow |5P_{1/2}, F' = 2\rangle$ transition. The sole purpose of this repump beam is to empty the $|5S_{1/2}, F = 1\rangle$ state and populate the $|5S_{1/2}, F = 2\rangle$ state. Henceforth we refer to this repump beam as the probe repump beam to distinguish it from the MOT repump beam.

To prepare the atom in the ground state of the closed cycling transition, i.e. $|5S_{1/2}, F = 2, m_F = -2\rangle$, we perform optical pumping by sending a σ_- beam tuned to the $|5S_{1/2}, F = 2\rangle \rightarrow |5P_{3/2}, F' = 2\rangle$ transition as well as the probe repump beam. The probe repump beam compensates for any excitation induced by the optical pumping beam that may cause the atom to decay to $|5S_{1/2}, F = 1\rangle$ state. The optical pumping beam will only induce optical transition that satisfies $\Delta m_F = -1$ selection rule while during spontaneous emission Δm_F can be either 0 or ± 1. If this process continues for a while, atom will eventually end up in $|5S_{1/2}, F = 2, m_F = -2\rangle$. This is a "dark state" that is effectively decoupled from the optical pumping beam because there is no corresponding $|5P_{3/2}, F' = 2, m_{F'} = -3\rangle$.

2.3 Experimental Setup

The main setup for the transmission experiment is shown in Fig. 2.2.

In this experiment, we use a circularly polarized dipole trap with a well-defined Gaussian spatial mode. The power of the dipole trap beam is locked in order to maintain a constant depth of the trapping potential. The presence of the dipole trap beam breaks the degeneracy among the m_F sublevels (AC Stark shift). It is therefore convenient to describe the atom with a quantization axis pointing along the z-axis (propagation direction of the dipole trap beam). With this quantization axis, the dipole trap beam is σ_+ polarized. To further break the degeneracy, a magnetic coil (not shown in Fig.2.2) is used to apply a small magnetic field of about 2 Gauss at the location of the atom along the z-axis.

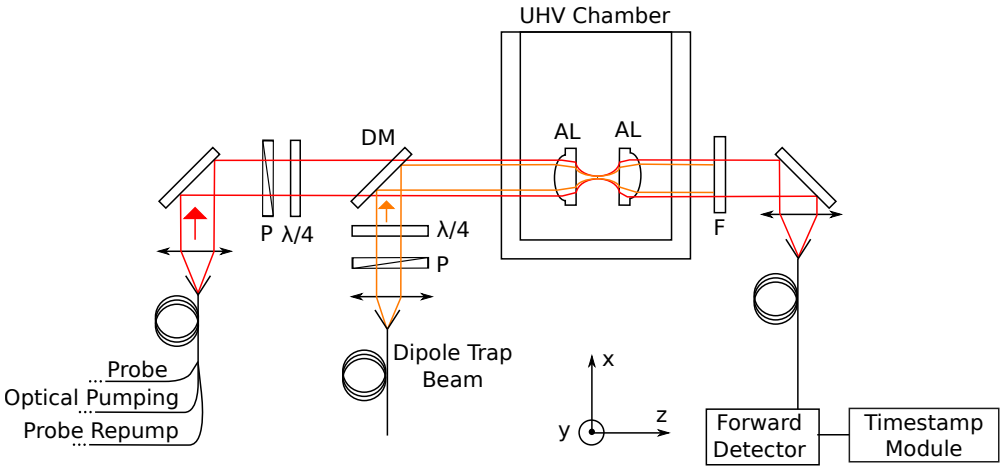

Figure 2.2: Experimental setup for the transmission experiment. P: polarizer, $\lambda/4$: quarter-wave plate, DM: dichroic mirror, AL: aspheric lens, UHV Chamber: ultra high vacuum chamber, F: interference filter that transmits light at 780 nm.

The probe beam and optical pumping beam are derived from separate external cavity diode lasers that are frequency-locked to the $|5S_{1/2}, F = 2\rangle \rightarrow |5P_{3/2}, F' = 1\rangle$ transition. The external cavity diode laser that produces the probe repump beam is locked to the transition between $|5S_{1/2}, F = 2\rangle$ and the cross-over resonance between $|5P_{1/2}, F' = 1\rangle$ and $|5P_{1/2}, F' = 2\rangle$. The frequency of each beam is then shifted using a separate Acousto-Optic Modulator (AOM) to match the intended frequency. The AOM also functions as a switch that controls if the beam

is sent to the atom. The optical pumping beam, probe beam, and probe repump beam are then coupled into optical fibers, combined and come out from a single fiber coupler. They are passed through a single mode optical fiber so that they have a well-defined Gaussian spatial mode at the atom. The polarizer and the quarter-wave plate ($\lambda/4$) transform each beam to a σ_- beam.

The excitation by the probe beam will make the atom fluoresce. A fraction of the atomic fluorescence is detected in the forward direction by the forward detector, a passively quenched silicon avalanche photodiode with a deadtime of about 3 μs and jitter time of about 1 ns. The timestamp module is used to record the arrival time of each photon detected by the photodetector with a timing resolution of about 125 ps.

During the loading of a single atom into the trap, the system will decide whether or not an atom has been trapped based on the detection counts in the forward detector.

The whole experiment is controlled by a pattern generator machine. It receives a series of command (the experimental sequence) from the computer and outputs a sequence of electrical signals. These electrical signals control the rest of the devices in the experimental setup.

2.4 Experimental Sequence

The experimental sequence for the transmission experiment is as follows (Fig. 2.3):

1. Load a single atom into the dipole trap by triggering on the signal detected by the forward detector.

2. Apply a bias magnetic field of 2 Gauss in the z direction at the site of the atom.

3. Perform state preparation by sending the optical pumping beam and the probe repump beam to the atom for 10 ms.

4. Turn off the optical pumping beam and turn on the probe beam. This is to allow some time for the optical pumping beam to be completely turned off and for the power of the probe beam to stabilize.

5. At this point in time the power of the probe beam has reached its steady state. The timestamp module starts recording the arrival time of each photon detected by the forward detector. This process lasts for 120 ms.

6. Turn off the magnetic field and the probe beam. Turn on the MOT cooling and MOT repump beams. Check if the atom is still there by measuring the power detected by the forward detector. If so, then repeat steps 2 to 6. Otherwise proceed to step 7 for background measurement.

7. At this point, there is no atom in the trap. Turn on the probe beam, probe repump beam and the magnetic field, wait for another 5 ms to allow them some time to stabilize.

8. The timestamp module starts recording the background signal in the forward detector in the absence of the atom. This process lasts for 2 s. At the end of the background measurement, return to step 1.

The background measurement gives the power level of the probe and probe repump beam in the absence of the atom. This is used as a reference that will be compared to the detected power in the presence of the atom.

2.5 Measurement of Transmission

The experimental sequence presented in Fig. 2.3 is repeated for different detunings of the σ_- probe beam with respect to the natural transition frequency (in the absence of dipole trap beam). Fig. 2.4 shows the average transmission at different detunings. The details on the averaging of the transmission value can be found in [8].

The lowest measured transmission is 94 %, corresponding to 6 % extinction. This is smaller than the 10 % extinction reported by [8] for the similar experimental parameters.

There are several reasons that can possibly explain why we observed a lower extinction value. Different input divergence of the probe beam can result in a weaker focusing by the aspheric lens. Also, any slight misalignment between the

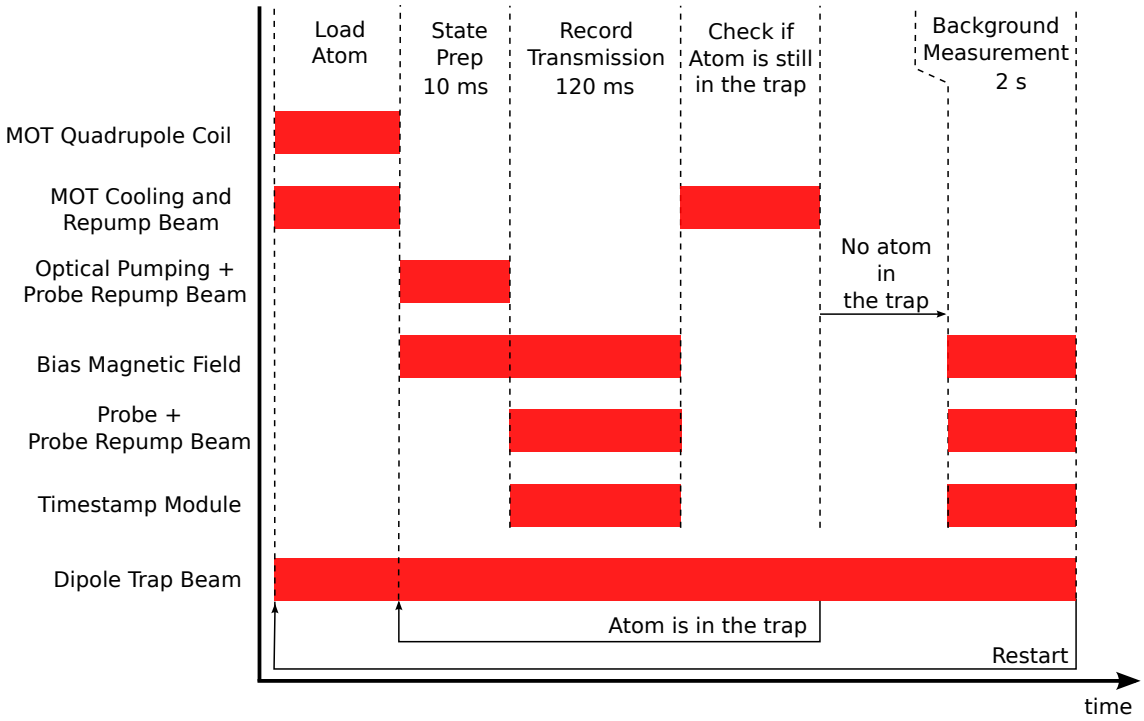

Figure 2.3: Schematic of the experimental sequence for the transmission experiment. Details in text.

probe beam and dipole trap beam can cause mismatch between the focus of the dipole trap beam (where the atom is) and the focus of the probe beam. Either of this will result in a slightly different probe electric field amplitude at the atom that may weaken the interaction between the atom and the probe beam [14]. Another possible explanation is that the MOT parameters in this experiment may not be optimal such that the temperature of the atomic cloud and hence the kinetic energy of the trapped atom is higher, causing it to wander off the focus more often. This results in weaker atom-light interaction and thus a lower extinction.

Despite the observed extinction being lower than the expected one, we can still measure the resonance frequency of the optical transition. The results of the transmission experiment indicate that the resonance frequency of the $|5S_{1/2}, F = 2, m_F = -2\rangle \rightarrow |5P_{3/2}, F' = 3, m_{F'} = -3\rangle$ transition is found at 76 MHz blue-detuned from the natural transition frequency.

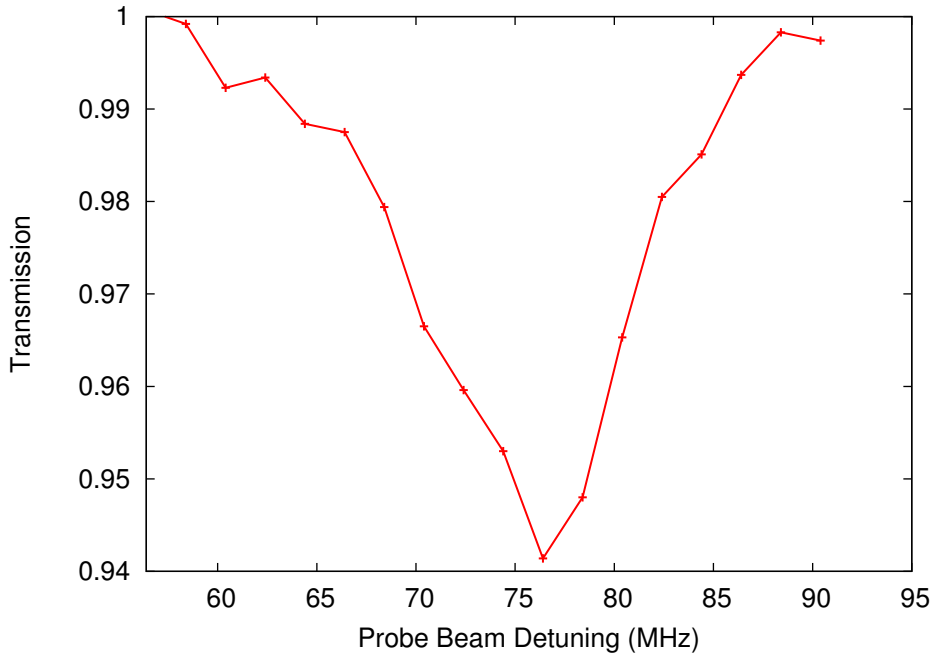

Figure 2.4: Average transmission of the (σ_-) probe beam across a trapped single ^{87}Rb atom measured as a function of its detuning with respect to the unshifted resonance frequency of $|5S_{1/2}, F = 2\rangle \rightarrow |5P_{3/2}, F' = 3\rangle$. The largest decrease in the transmission value corresponds to the resonance frequency of the probed optical transition ($|5S_{1/2}, F = 2, m_F = -2\rangle \rightarrow |5P_{3/2}, F' = 3, m_{F'} = -3\rangle$).

3

Pulsed Excitation Experiment

3.1 Aiming for a π Pulse

In the previous chapter, we presented the closed cycling transition in ^{87}Rb atom that can be approximated as an effective two-level system. The electric dipolar interaction between the probe light and the two-level system causes the state of the atom to undergo Rabi oscillation between the ground and excited state of the two-level system (refer to the Appendix A1).

Our goal is to generate a spontaneously emitted single photon from a single atom with a high probability. This can be done by sending an optical pulse to excite the atom with a high excitation probability. Excitation probability here is defined as the probability of the atom being in the excited state once an optical pulse excites it.

To achieve a high excitation probability, we need to make sure that the optical pulse brings the atom just right to the excited state. Assuming that the atom starts from the ground state of the two-level system, the optical pulse will have to bring the atom to the first maximum of the Rabi oscillation. This corresponds to

$$\int_0^T \Omega(t)dt = \pi\,, \tag{3.1}$$

where $\Omega(t) = -\left(\vec{d}_{ge} \cdot \vec{\epsilon}\right) E_0(t)/\hbar$ is the instantaneous Rabi frequency and T is the duration of the optical pulse. This is referred to as a π pulse.

In this experiment, we choose to send a rectangular optical pulse. The optical frequency of this optical pulse has been determined through the transmission experiment detailed in the previous chapter. The duration of the optical pulse has to be much shorter than the lifetime of the excited state ($\tau_e \approx 27\,\text{ns}$) to minimize decay from the excited state during the excitation process. The strategy is to fix the duration of the optical pulse and to vary its amplitude such that a π pulse is achieved.

The organization of this chapter is as follows: we first present an overview of the optical pulse generation. Next, we present the experimental setup and show how the optical pulse can be characterized using a single photon detector. Finally, we present the experimental sequence and the results. We will also briefly discuss another excitation method using chirped pulses.

3.2 Optical Pulse Generation

3.2.1 Fast Amplitude Modulator

The intended optical pulse is a rectangular pulse with a duration T much smaller than τ_e and with very well defined edges (rise and fall time $\lesssim 1\,\text{ns}$). The latter is to make sure that we have a clear separation between the spontaneous emission regime and the excitation process.

One method to generate an optical pulse is to use an Acousto-Optic Modulator (AOM) that is currently used as a switch as well as to tune the optical frequency of the probe beam. However, since AOMs rely on acoustic waves to modulate the beam, they are in practice not fast enough to be used for such high speed pulse modulation (rise and fall time in the order of 100 ns). As such, the AOM is not suitable for very fast switching purpose.

Another alternative is to use an Electro-Optic Modulator (EOM) as the amplitude modulator. The EOM we use is an EOSPACE 20 GHz broadband Mach-

Zehnder based interferometric modulator with an extinction ratio[1] of $\sim 21\,\mathrm{dB}$. The EOM is enclosed in a metallic cage that is temperature stabilized at $35\,^{\circ}\mathrm{C}$. This reduces the effects of external influences such as the room's temperature fluctuations.

The amplitude modulation works by modulating the phase using electro-optic effect in one of the interferometer's arms. The EOM possesses separate DC bias and broadband RF ports on which the modulation signal can be applied. The DC bias port is used to set the operating point of the modulation. The RF port is where the fast modulation signal is applied. Fig. 3.1 shows the transmission of the EOM for different values of DC bias voltage (with zero voltage on the RF port). The π-voltage (V_π) is the change in the voltage required to go from the minimum to the maximum transmission point of the EOM. Note that the V_π for the DC bias port is different from V_π for the RF port, we denote them by $V_{\pi,DC}$ and $V_{\pi,RF}$[2].

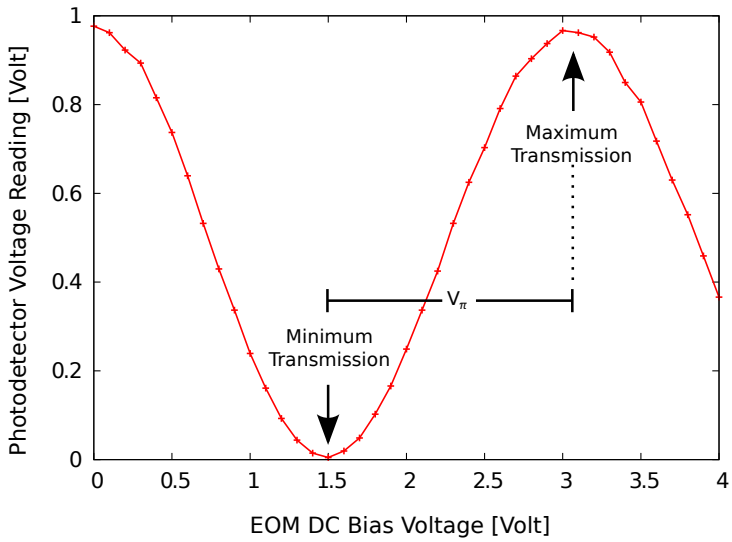

Figure 3.1: Optical output power from the EOM measured by a Hamamatsu S5107 Si PIN Photodiode as a function of the DC bias voltage with no RF input. The vertical axis is the voltage reading on the photodetector that is proportional to the detected optical power.

[1]Given an input with constant power, the extinction ratio is defined as the ratio between the maximum and the minimum transmission of the amplitude modulator

[2]In fact the V_π is a function of the modulation frequency.

In our experiment, we set the DC bias voltage such that the EOM is at the minimum transmission point with no RF input. During the application of $V_{\pi,RF}$ at the RF port, the EOM will shift to the maximum transmission point. Therefore to obtain an optical pulse, we apply $V_{\pi,RF}$ at the RF port of the EOM for the intended duration of the optical pulse.

Although the EOM has been temperature stabilized, the DC bias voltage needed to position the EOM at the minimum transmission point drifts in the timescale of half an hour. Therefore during the experiment, the DC bias voltage of the EOM is recalibrated every 15 to 20 minutes.

To minimize the amount of light transmitted by the amplitude modulator when it is at its minimum transmission point (the base floor noise when we are not sending optical pulses), we decided to use two EOMs in series. The combination of two EOMs will result in an extinction ratio of $\approx$ 40 dB for the amplitude modulation. Fig. 3.2 shows the schematic of the optical pulse generation in the two EOM configuration.

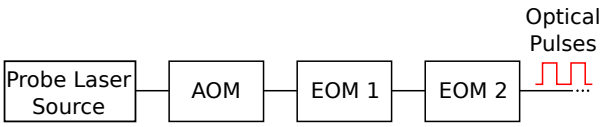

Figure 3.2: Schematic of the optical pulse generation process.

3.2.2 Overview of the Electrical Pulse Generation

The shape of the optical pulse depends on the shape of the electrical RF input. Therefore, we need to generate short electrical pulses with well defined edges. As the shortest duration of the electrical pulse that our pattern generator can generate is 20 ns, some additional electronics are needed in order to generate an electrical pulse shorter than 20 ns.

The schematic for the electrical pulse generation is shown in Fig. 3.3. The 20 ns electrical pulse generated by the pattern generator is duplicated by an electronic fanout unit producing two identical electrical pulses, both of which enter an electronic delay unit that delays one of them with respect to the other with a resolution of $\sim$ 10 ps. The coincidence unit acts as a coincidence gate that

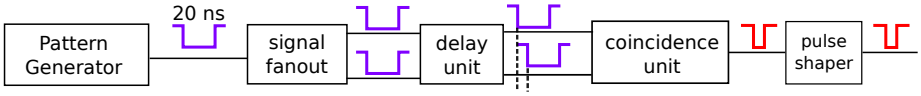

Figure 3.3: Schematic of the electrical pulse generation process.

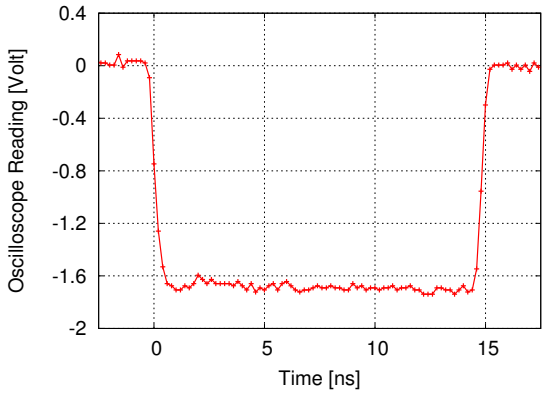

Figure 3.4: A 15 ns electrical pulse at the output of the pulse shaper unit with a negative amplitude.

produces an electrical pulse with a duration defined by the relative delay of the input pulses. The electrical pulse then enters a pulse shaper unit that shortens the rise and fall time to about 1 ns. An example of a 15 ns electrical pulse at the output of the pulse shaper unit is shown in Fig. 3.4.

In the two EOM configuration, each EOM is now controlled by a separate set of delay, coincidence and pulse shaper units. The two EOM configuration demands that the second EOM is turned on only when the optical pulse generated by the first EOM arrives at the second EOM. This implies that the first EOM must receive the electrical pulse earlier than the second EOM. This is made possible because the delay unit for each EOM can be tuned independently of the other.

3.3 Experimental Setup

Fig. 3.5 shows the main setup used in the pulsed excitation experiment. This setup is similar to the setup in transmission experiment (Section 2.3) with the addition of a few components.

As the forward detector is a single photon detector, a neutral density filter

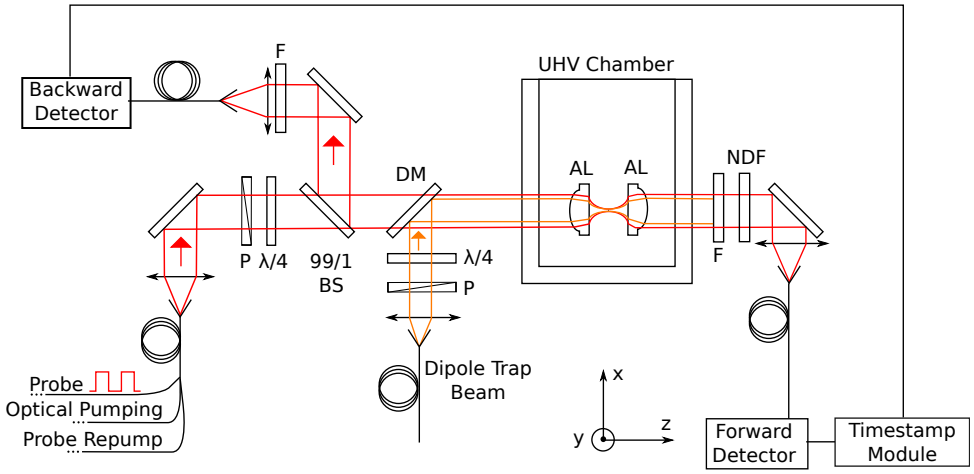

Figure 3.5: Experimental setup in the pulsed excitation experiment. P: polarizer, $\lambda/4$: quarter-wave plate, 99/1 BS: beam splitter that reflects 99% and transmits 1% of the incident beam, DM: dichroic mirror, AL: aspheric lens, UHV Chamber: ultra high vacuum chamber, F: interference filter that transmits light at 780 nm, NDF: neutral density filter.

(NDF) is added just before the forward detector to prevent saturation due to the optical pulse. The NDF attenuates the optical pulse to the point that on average only $\approx 1\%$ of the photons in the optical pulse reaches the forward detector.

With the presence of NDF in the forward detection arm, the forward detector will only detect a negligible amount of the atomic fluorescence. Therefore, we detect the atomic fluorescence using another single photon detector in the backward direction (backward detector in Fig. 3.5).

During the loading of a single atom into the trap, the system will decide whether or not an atom has been trapped based on the detection counts in the backward detector. The single photon emission from the atom during the pulsed excitation experiment will also be measured by the backward detector.

3.4 Optical Pulse Characterization

Before sending the optical pulse to the atom, the optical pulses are characterized by reconstructing their shape using the forward detector. From this, we can get an estimate of the average number of photons per optical pulse incident at the

atom.

3.4.1 Optical Pulse Reconstruction Using a Single Photon Detector

Fig. 3.6a shows an example of a 3 ns optical pulse reconstructed in the forward detector (passively-quenched avalanche photodiode with a timing jitter of ~ 1 ns). The neutral density filter attenuates the optical pulse by 37 dB. As we are limited by the jitter of the single photon detector (about 1 ns), the data is processed in 1 ns timebins. The vertical axis shows the normalized counts at time t, $N(t)$. It is defined as

$$N(t) = \frac{\text{Number of clicks in the detector at time } t}{\text{Number of optical pulses}}$$

Fig. 3.6b shows the detection events in the backward detector. There is a small fraction of optical pulse back-reflected towards the backward detector. As we will be detecting the spontaneously emitted photon using the backward detector, the falling edge of this back-reflection will serve as the timing reference that marks beginning of the spontaneous emission.

3.4.2 The Average Number of Photons per Pulse

The area under the graph shown in Fig. 3.6 is equal to the average number of photons per pulse detected by the detector. The average number of photons per pulse (denoted as N_p) incident on the atom can be calculated by accounting for all relevant losses from the atom to the detector. We demonstrate it here by taking the data in Fig. 3.6a as our example.

The dominant losses from the atom to the forward detector can be attributed to the neutral density filters ($\sim$37 dB), coupling efficiency into the fiber ($\sim$70%) and the quantum efficiency of the single photon detector ($\sim$ 50%). This results in a total transmission factor of 7.0×10^{-5} with an uncertainty roughly estimated to be 1×10^{-5}.

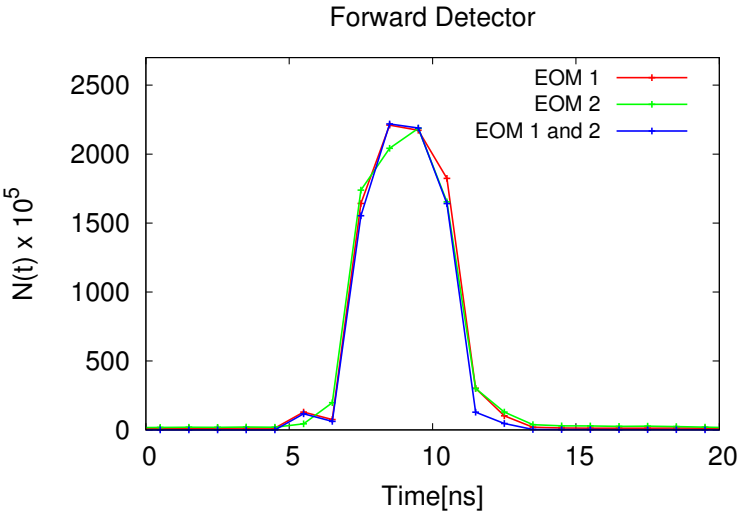

(a)

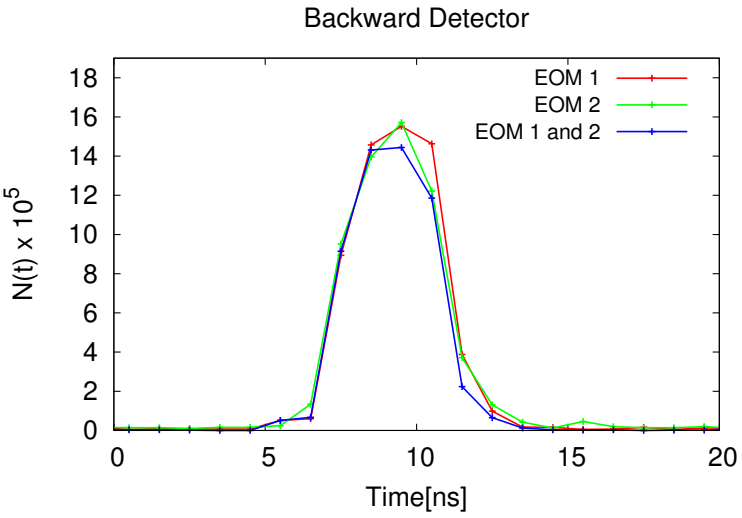

(b)

Figure 3.6: Optical pulse reconstruction in the forward and backward detectors. Both are passively-quenched avalanche photodiodes. (EOM1) the first EOM is used for modulation while the second EOM is set at the maximum transmission point. (EOM2) the second EOM is used for modulation while the first EOM is set at the maximum transmission point. (EOM 1 and 2) Both EOMs are used for modulation. The fact that the reconstructed optical pulses coincide with each other demonstrates that we have successfully synchronized the two EOMs.

Therefore the average number of photons per pulse incident on the atom is equal to the average number of photons per pulse detected by the forward detector divided by the total transmission factor. This results in an average of $\sim 1140 \pm 160$ photons per optical pulse incident on the atom for the optical pulse in Fig. 3.6.

3.5 Experimental Sequence

The experimental sequence for the pulsed excitation experiment is as follows (Fig. 3.7):

1. Load a single atom into the trap by triggering on the signal detected by the backward detector.
2. Perform molasses cooling for 10 ms to further cool down the atom in the trap.
3. Apply a small bias magnetic field of 2 Gauss in the z-direction. Perform state preparation for 10 ms by sending the optical pumping and probe repump beams to the atom. This step prepares the atom in the $|5S_{1/2}, F = 2, m_F = -2\rangle$ state.
4. Send a signal to the EOMs to generate an optical pulse and let the timestamp module records the arrival time of each event detected in the forward as well in the backward detector for 2 μs.
5. Repeat step 4 every 10 μs for 100 times.
6. Check if the atom is still in the dipole trap. If so, then repeat steps 2 to 5. Otherwise, restart from step 1.

3.6 Spontaneous Emission from a Single Atom

Fig. 3.8 shows the detection events in the backward detector in the pulsed excitation experiment with a 3 ns optical pulse. As expected, with atom in the trap, the backward detector detects the atomic fluorescence.

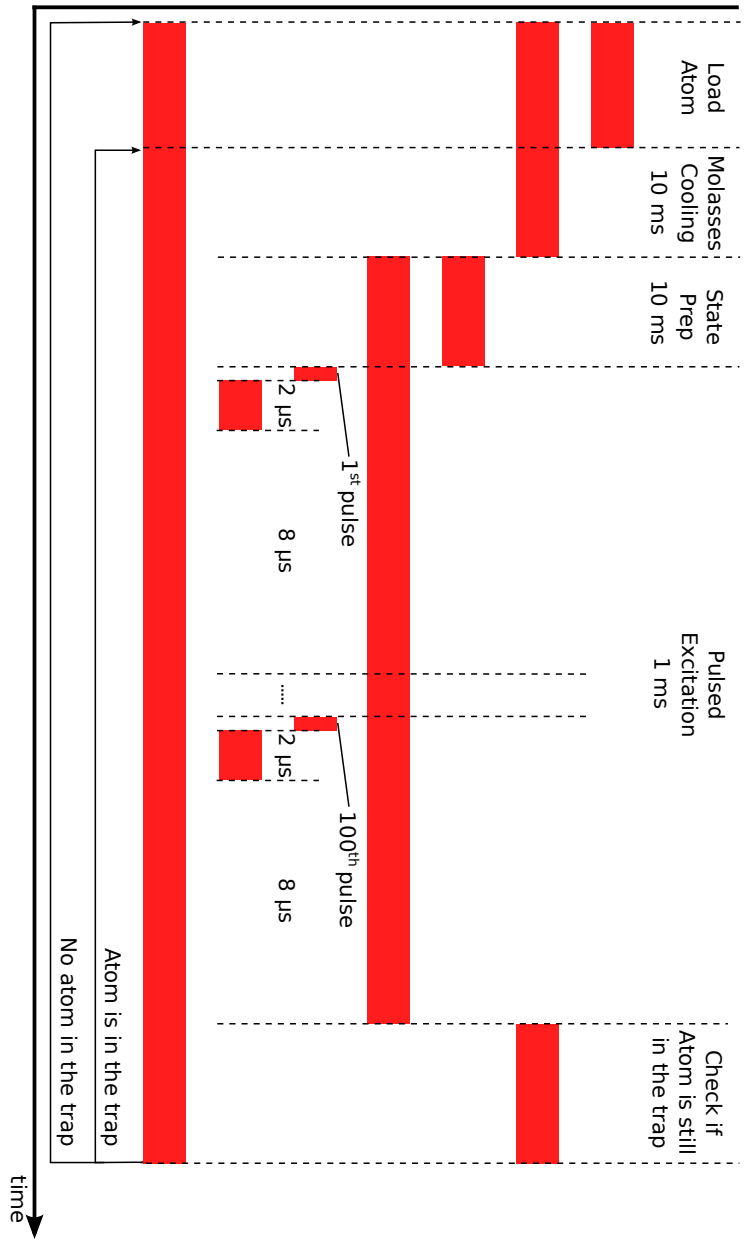

Figure 3.7: The experimental sequence for the pulsed excitation experiment. Details in text.

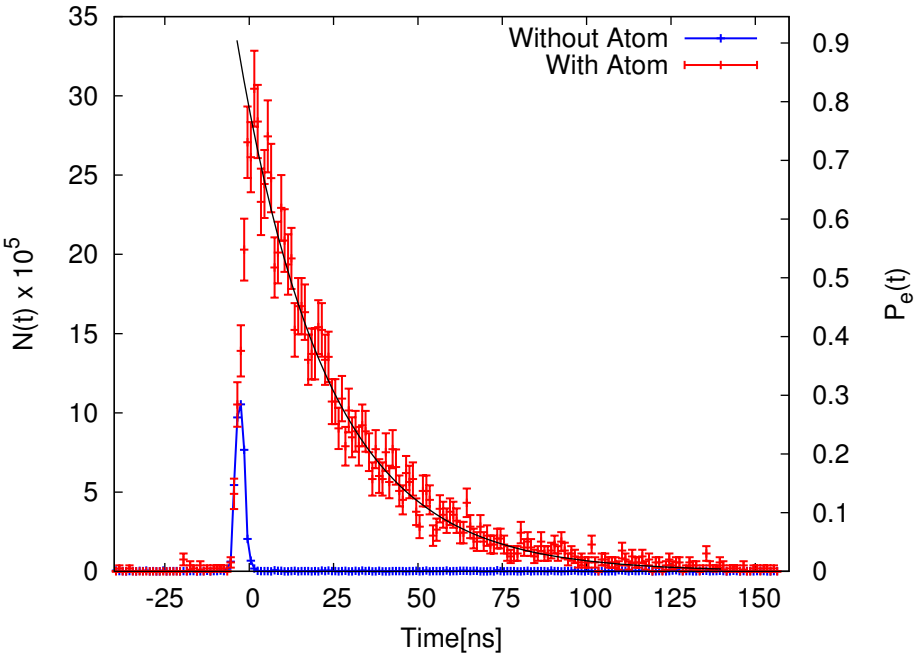

Figure 3.8: ("Without Atom") Detection events in the backward detector without atom in the trap. The detector measures the back-reflected optical pulse. ("With Atom") Detection results from the backward detector during the pulsed excitation experiment with an average of 700 photons per 3 ns optical pulse incident on the atom. The detector measures the atomic fluorescence as well as the back-reflected optical pulse. The left axis indicates the normalized counts, $N(t)$, and the right axis indicates the probability of the atom being in the excited state, $P_e(t)$. The displayed error bar is the standard deviation of each data point attributed to the Poissonian counting statistics. The black line is an exponential fit with a characteristic decay time of 26.5 ± 0.5 ns.

The time axis of the data has been shifted such that $t = 0$ coincides with the falling edge of the optical pulse. The negligible amount of atomic fluorescence before the optical pulse demonstrates that the base floor outside the optical pulses has been heavily suppressed. Otherwise, we would see a non-negligible amount of atomic fluorescence even before the optical pulse. This means that all the detection events after $t = 0$ (excluding the small contribution due to the dark counts) can be attributed to the spontaneously emitted photons from the atom.

An exponential fit to the spontaneous emission curve gives a characteristic time decay of 26.5 ± 0.5 ns for the $5P_{3/2}$ state, in agreement with the results reported in the literatures, i.e. 26.24 ± 0.04 ns [15], 26.47 ± 0.30 ns [16], 27.1 ± 1.4 ns

[17].

From the fluorescence data shown in Fig. 3.8, it is also possible to infer the probability of the atom being in the excited state as a function of time, denoted as $P_e(t)$. The probability of the atom being in the excited state decays due to spontaneous emission according to the relation (see Appendix A2)

$$\frac{dP_e(t)}{dt} = -\Gamma P_e(t)$$

The rate of change of $P_e(t)$ can be calculated from the number of photons emitted at time t within the 1 ns timebin (Δt).

$$\begin{aligned} P_e(t) &= -\frac{1}{\Gamma}\frac{dP_e(t)}{dt} \\ &\approx -\frac{1}{\Gamma}\frac{P_e(t+\Delta t) - P_e(t)}{\Delta t} \\ &\approx \frac{1}{\Gamma}\frac{N(t)}{\eta_d \eta_s \Delta t} \end{aligned}$$

η_d is the detection efficiency (estimated to be 0.3) and η_s is the spatial overlap parameter (measured to be 0.03). The detection efficiency includes the coupling efficiency into the fiber coupler and the quantum efficiency of the APD. The spatial overlap parameter is a measure of the overlap between the collection mode and the emission mode of the atom.

3.7 Rabi Oscillation

3.7.1 Excitation Probability vs Average Number of Photon

The total excitation probability, P_E can be extracted from the fluorescence data by integrating the normalized counts $N(t)$ under the spontaneous emission regime

and dividing it by the overall detection and collection efficiency $(\eta_d \cdot \eta_s)$.

$$P_E = \frac{\int_{t_i}^{t_f} N(t)dt}{\eta_d \cdot \eta_s} = \frac{A(t_i, t_f)}{\eta_d \cdot \eta_s} \tag{3.2}$$

We choose $t_i = 0$ to coincide with the end of the optical pulse and $t_f = 155\,\text{ns}$ which corresponds to approximately $5.7\tau_e$ away from the t_i, where $\tau_e \approx 27\,\text{ns}$. This is motivated by the fact that for $t > t_f$, the noise is more dominant than the signal. In addition, $e^{-(t_f - t_i)/\tau_e} \approx 10^{-3}$ and the tail of the exponential decay starting from t_f only contributes about 0.1 % to the total excitation probability. This justifies the choice of neglecting the tail of this exponential decay.

Fig. 3.9 shows the dependence between the total excitation probability (P_E) extracted from the fluorescence data and the average number of photons (N_p) for a 3 ns optical pulse. We do not exceed $N_p \approx 1600$ as we are limited by the maximum power that can be obtained from our laser.

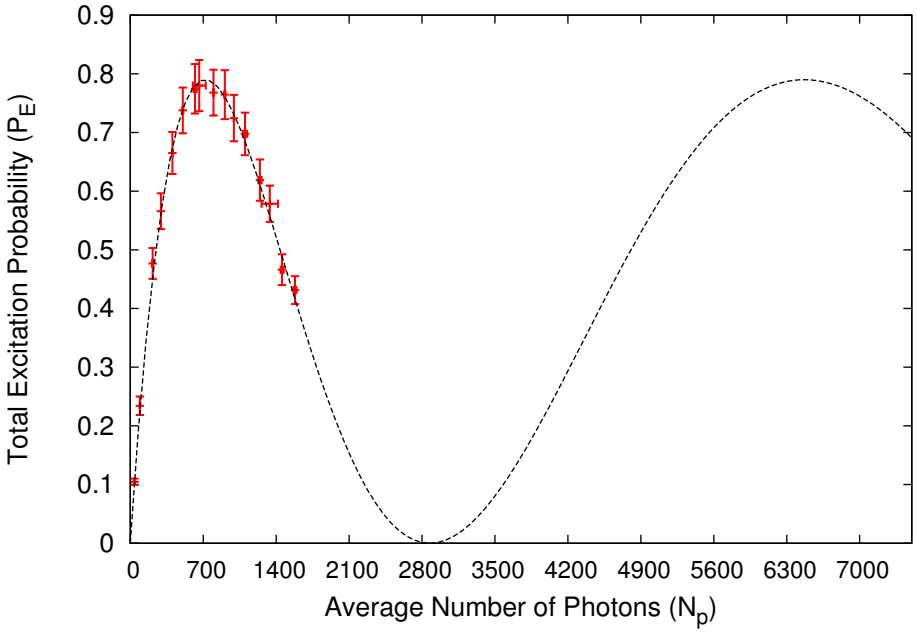

Figure 3.9: (Red data points) Total excitation probability versus average number of photons per 3 ns optical pulse incident at the atom. (Dashed line) Fit of $A\sin^2(\sqrt{N_p}B)$ where A and B are the fitted parameters. Refer to (3.4) in the main text for more details.

The uncertainty of the average number of photons shown in Fig. 3.9 is the difference between average number of photons measured before and after each data point. This difference is mainly attributed to the drift in the power of the probe laser that is only frequency-locked.

The uncertainty in the total excitation probability (ΔP_E) shown in Fig. 3.9 consists of the uncertainty due to the Poissonian counting statistics (ΔP_{poiss}) and also the timing uncertainty (ΔP_t).

$$\Delta P_E = \Delta P_{poiss} + \Delta P_t$$

The timing uncertainty is attributed to the jitter time of the detector itself that is in the order of 1 ns. This causes an error in the determination of t_i and t_f. ΔP_t is calculated as follows:

$$\Delta P_t = \frac{1}{\eta}\sqrt{\sigma_{t_i}^2\left(\frac{\partial A(t_i,t_f)}{\partial t_i}\right)^2 + \sigma_{t_f}^2\left(\frac{\partial A(t_i,t_f)}{\partial t_f}\right)^2}, \tag{3.3}$$

where σ_{t_i} and σ_{t_f} are the timing uncertainties (1 ns). The partial derivatives are calculated by discretizing each of them in time. Due to the choice of t_f, the contribution of the second term in ΔP_t is negligible with respect to the first term. Therefore, ΔP_t approximates to

$$\begin{aligned}\Delta P_t &\approx \frac{1}{\eta}\sigma_{t_i}\left(\frac{\partial A(t_i,t_f)}{\partial t_i}\right)\\ &\approx \frac{1}{\eta}\times 1\text{ ns}\times\frac{1}{2}\left(\frac{|A(t_i-1\text{ ns},t_f)-A(t_i,t_f)|}{1\text{ ns}}+\frac{|A(t_i+1\text{ ns},t_f)-A(t_i,t_f)|}{1\text{ ns}}\right)\end{aligned}$$

3.7.2 π Pulse

The total excitation probability reaches a maximum of 78±4 % for $N_p = 700$. This is the π pulse for a 3 ns optical pulse.

There are several reasons for which the total excitation probability does not reach 100 %. First of all, as the atom is excited by a 3 ns optical pulse, the free decay of the excited state imposes a theoretical maximum of $\frac{1}{2}(1+e^{-3/27}) \approx 94.7\,\%$

for the total excitation probability.

Also, in the calculation of the total excitation probability, we did not specify the uncertainty in the overall collection and detection efficiency ($\eta_d \cdot \eta_s$). It is known that the quoted value of spatial overlap parameter η_s has a large uncertainty. One way to calibrate the overall detection and collection efficiency is to compare the saturated photon emission rate of the probed transition under a continuous excitation with the measured count rate [18].

Furthermore, as the probe beam has a gaussian spatial profile at the site of the atom, any thermal motion of the atom around the focus of the lens can change the amplitude of the electric field at the atom. Consequently, the atom may not always experience a π pulse every time and this makes the excitation process less efficient. This effect accumulates over many cycles of excitation and this is reflected in the total excitation probability that is effectively reduced.

3.7.3 Discussion

Fig. 3.9 is an unconventional way of describing a Rabi oscillation. Usually, Rabi oscillation is described in the temporal domain where the excitation probability varies sinusoidally as a function of the optical pulse duration T (fixed amplitude of the optical pulse, i.e. constant Rabi frequency Ω_1. Refer to Appendix A1).

$$P_E = \sin^2\left(\frac{\Omega_1}{2}T\right)$$

Here, it is the amplitude of the optical pulse that is varied for a fixed optical pulse duration. As the Rabi frequency is proportional to the square root of the average number of photons, therefore

$$P_E = \sin^2\left(\sqrt{N_p} \times \text{constant}\right) \tag{3.4}$$

The dashed line in Fig. 3.9 is the theoretical fit of the (3.4) to the data.

3.8 Alternative Excitation Method

An alternative way to excite an atom is through adiabatic rapid passage (ARP) [11, 19] via chirped pulses. In this method, frequency of the excitation light is initially tuned below (or above) resonance and adiabatically swept through the resonance. The process has to be much faster than the lifetime of the excited state. At the same time, it has to be slow enough such that the atom is still able to follow the change adiabatically.

In the picture of Bloch sphere, suppose that the ground and excited states of the two-level atom are represented by positive and negative z-axis. The state of the atom initially in the ground state can be represented by a Bloch vector pointing in the positive z-axis. With the excitation light initially far-detuned, the Bloch vector starts rotating around an axis nearly parallel to the z-axis. As the detuning of the excitation light is slowly swept through resonance, the rotation axis of the Bloch vector slowly passes through the xy-plane and ends up nearly parallel to the z-axis, this time pointing in the negative z-axis. The Bloch vector itself will slowly follow the movement of the rotation axis and eventually point in the negative z-axis as well. Thus atom initially in the ground state is left in the excited state after the excitation with very high probability.

ARP was first introduced and performed in the domain of nuclear magnetic resonance [20]. It was first demonstrated in the optical regime in which the frequency of the excitation light is fixed and the resonant frequency of the molecular system is varied via Stark effect [21].

The excitation method we use in this work relies on a π pulse that is sensitive to the position of the atom as well as the intensity fluctuation of the excitation light. The ARP method is insensitive to these two factors. The downside of ARP is that it requires extremely fast chirp and more power than a π pulse.

4

Conclusion and Ongoing Work

4.1 Conclusion

We have demonstrated that we can generate a single photon from a trapped single atom with a high excitation probability. This is done by exciting the single atom with an optical pulse along a closed cycling transition ($|5S_{1/2}, F = 2, m_F = -2\rangle \rightarrow |5P_{3/2}, F' = 3, m'_F = -3\rangle$).

To achieve a high excitation probability, we proceeded in two steps. First, we measured the resonance frequency of the optical transition that we want to excite. The resonance frequency of the optical transition corresponds to the largest decrease in the transmission of the probe beam. It was found to be at around 76 MHz detuning from the natural transition frequency of the closed cycling transition. Second, we chose a particular duration of optical pulse and varied the average number of photons per optical pulse such that we achieved a π pulse. For a rectangular optical pulse of 3 ns duration, the optical pulse achieved the highest excitation probability of $78 \pm 4\,\%$ for an average of 700 photons per optical pulse incident at the atom.

4.2 Towards Interfering Single Photons from Different Systems

With the single atom setup ready to produce a spontaneously emitted single photon through π pulse excitation, we can proceed to interfere this single photon with the heralded single photon of an entangled photon pair produced through four wave mixing process in ^{87}Rb atomic ensemble [9].

We have aligned the Hong-Ou-Mandel interferometer setup (Fig. 4.1) that will be used to observe the quantum interference between the two single photon. The next task is to come up with the exact timing sequences that will include both setups.

The scheme for the joint experiment is as follows: upon receiving a signal that a heralded single photon has been generated by the atomic ensemble setup, we wait for a calibrated delay time before sending an optical pulse to the single atom to generate a single photon through spontaneous emission. We hope to observe the Hong-Ou-Mandel interference as the wavepacket of each photon interferes at the 50:50 beam splitter.

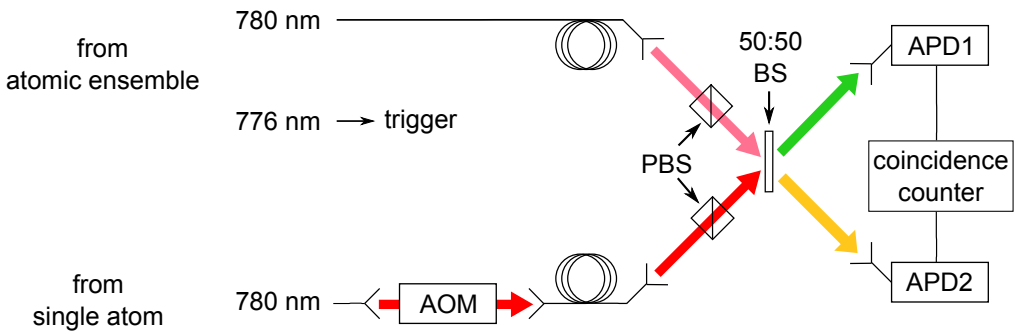

Figure 4.1: Schematic of the Hong-Ou-Mandel interferometer setup. The spontaneously emitted 780 nm single photon from a trapped single atom and the heralded 780 nm single photon from an entangled photon pair (the 776 nm photon being the trigger) produced through four wave mixing process in an atomic ensemble interfere at the 50:50 beam splitter (BS). The acousto-optic modulator (AOM) compensates for the frequency difference due to the AC Stark shift induced by the presence of the dipole trap beam. The polarising beam splitters (PBS) ensure that the two photons have the same polarisation. The coincidence counter measures the coincidence between the detection events measured by the avalanche photo diodes (APD) at the output ports of the beam splitter.

Appendix A

Theory of Atom-Light Interaction

The subject of atom-light interaction has been discussed in great detail in [22, 23]. The treatment presented here follows closely [23].

Here, we will restrict our discussion to the description of an atom as a two-level system. Although this is not typically the case in real atoms, some elements do possess closed cycling transitions. This allows us to approximate a multi-level atom as an effective two-level system.

In the first part, we examine the dynamics of a two-level system in the presence of external light. In the second part, we examine the situation where an excited two-level system in the absence of external light decays to the ground state due to the interaction with the vacuum radiation modes.

A.1 Excitation of a Two-Level System

Consider the following problem of an electron in a two-level system interacting with excitation light as shown in Fig. A.1.

The transition frequency between the ground state $|g\rangle$ and the excited state $|e\rangle$ is denoted as $\omega_0 = |E_e - E_g|/\hbar$. The electric field of the excitation light is assumed to be of the form $\vec{E}(t) = E_0 \cos(\omega t)\vec{\epsilon}$, with frequency ω, polarization vector $\vec{\epsilon}\,(|\vec{\epsilon}| = 1)$ and is treated as a classical field for simplicity. We use the long-wavelength or dipole approximation where the light's wavelength is assumed to

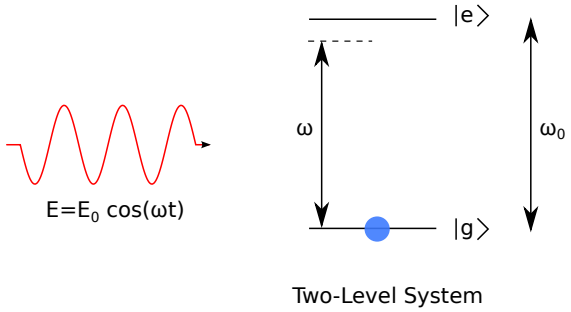

Figure A.1: Two-level system interacting with light.

be much larger than the size of the atom. In this approximation, the amplitude of the excitation light over the atom can be approximated as a constant, E_0.

The total hamiltonian of the two-level system under the dipole approximation is

$$\hat{H} = \hat{H}_{atom} + \hat{H}_{dip} \tag{A.1}$$

,where the atomic free-evolution hamiltonian is

$$\hat{H}_{atom} = \hbar\omega_0 |e\rangle\langle e|$$

The energy levels are defined such that the ground state has zero energy. The dipolar interaction hamiltonian is

$$\begin{aligned} \hat{H}_{dip} &= -\hat{\vec{d}} \cdot \vec{E}(t) \\ &= -\left(\hat{\vec{d}} \cdot \vec{\epsilon}\right) E_0 \cos(\omega t) \end{aligned}$$

The atomic dipole operator is the product between the charge of the electron and the position operator of the electron, i.e. $\hat{\vec{d}} = -e\hat{\vec{r}}_e$. In the eigenstates of the free-evolution hamiltonian, the atomic dipole operator can be expressed as

$$\hat{\vec{d}} = \left[\vec{d}_{ge}\right] |g\rangle\langle e| + \left[\vec{d}_{ge}\right]^* |e\rangle\langle g|$$

, where $\vec{d}_{ge} = \langle g|\hat{\vec{d}}|e\rangle$ is nonvanishing only if $|e\rangle$ and $|g\rangle$ are of opposite parity. Here, the matrix element $\vec{d}_{ge}$ is chosen to be real.

The state of the atom at any later time t, i.e. $|\psi(t)\rangle$, can also be expressed as

$$|\psi(t)\rangle = c_g(t)|g\rangle + c_e(t)e^{-i\omega_0 t}|e\rangle \tag{A.2}$$

The coefficients $c_g(t)$ and $c_e(t)$ can be found by solving the Schrödinger equation using the hamiltonian in (A.1) and the state decomposition above (A.2). In the rotating wave approximation, i.e. $|\omega - \omega_0| \ll (\omega + \omega_0)$, the Schrödinger equation reduces to

$$i\hbar\frac{d|\psi(t)\rangle}{dt} = \hat{H}|\psi(t)\rangle \rightarrow \left\{ \begin{array}{l} i\hbar\dfrac{dc_g(t)}{dt} = \dfrac{\Omega_1}{2}c_e(t)e^{i(\omega-\omega_0)t} \\ \\ i\hbar\dfrac{dc_e(t)}{dt} = \dfrac{\Omega_1}{2}c_g(t)e^{-i(\omega-\omega_0)t} \end{array} \right\}$$

, with $\Omega_1 = \left(\vec{d}_{ge}\cdot\vec{\epsilon}\right)E_0/\hbar$ being defined as the *Rabi frequency* and is defined such that $\Omega_1 > 0$. Note that the Rabi frequency is proportional to the amplitude of the electric field.

Define the detuning of the external light with respect to the atomic transition as $\Delta\omega := \omega - \omega_0$. The solution to the coupled differential equations above for an arbitrary initial state $(c_g(0), c_e(0))$ is

$$\begin{aligned} c_g(t) &= e^{i\Delta\omega t/2}\left[c_g(0)\cos\left(\frac{\Omega}{2}t\right) - \frac{i}{\Omega}\left(c_e(0)\Omega_1 + c_g(0)\Delta\omega\right)\sin\left(\frac{\Omega}{2}t\right)\right] \\ c_e(t) &= e^{-i\Delta\omega t/2}\left[c_e(0)\cos\left(\frac{\Omega}{2}t\right) - \frac{i}{\Omega}\left(c_g(0)\Omega_1 + c_e(0)\Delta\omega\right)\sin\left(\frac{\Omega}{2}t\right)\right] \end{aligned} \tag{A.3}$$

, with $\Omega = \sqrt{\Omega_1^2 + \Delta\omega^2}$ defined as the generalized Rabi frequency.

In the following, we illustrate three special cases that are of interest to us.

Example 1: For a two-level system initially prepared in the ground state $(c_g(0) = 1, c_e(0) = 0)$ and excitation light of constant amplitude, the probability

of finding the system in the excited state as a function of time is

$$P_e(t) = |c_e(t)|^2 = \frac{\Omega_1^2}{\Omega^2} \sin^2\left(\frac{\Omega}{2}t\right)$$

The population of the excited state oscillates with frequency Ω. This oscillation is usually referred to as the *Rabi oscillation*. The maximum value of $P_e(t)$ occurs when $\Omega T = \pi$ for a value of $P_{e,max} = \Omega_1^2/\Omega^2$ which is equal to 1 for excitation light at resonant with the transition frequency. An optical pulse of this duration ($T = \pi/\Omega$) is usually referred to as a π pulse. In other words, a π pulse is the shortest optical pulse required to achieve the highest probability of the atom being in the excited state.

Example 2 : If the atom is initially prepared in the excited state ($c_g(0) = 0, c_e(0) = 1$), then the probability of the atom being in the ground state is

$$P_g(t) = \frac{\Omega_1^2}{\Omega^2} \sin^2\left(\frac{\Omega}{2}t\right) \tag{A.4}$$

In particular, this result predicts that the atom will stay in the excited state forever if there is no excitation light for $t \geq 0$.

Example 3: Consider the special case where the excitation light is on resonance with the transition frequency ($\Delta\omega = 0$). If the amplitude of the light slowly fluctuates in time, ie. $\Omega_1 = \Omega_1(t)$, the requirement to get the π pulse can be generalized to

$$\int_0^T \Omega_1(t)dt = \pi$$

To illustrate this, consider the evolution of the atomic state interacting with an excitation light at resonance for an infinitesimal time step dt at time t. During this time interval, the Rabi frequency can be regarded as a constant. The coefficients

$c_g(t+dt)$ and $c_e(t+dt)$ in (A.3) can be expressed as

$$\begin{pmatrix} c_g(t+dt) \\ c_e(t+dt) \end{pmatrix} = \underbrace{\begin{pmatrix} \cos\left(\frac{\Omega_1(t)}{2}dt\right) & -i\sin\left(\frac{\Omega_1(t)}{2}dt\right) \\ -i\sin\left(\frac{\Omega_1(t)}{2}dt\right) & \cos\left(\frac{\Omega_1(t)}{2}dt\right) \end{pmatrix}}_{\left[\hat{U}(t,t+dt)\right]} \begin{pmatrix} c_g(t) \\ c_e(t) \end{pmatrix}$$

The matrix $\left[\hat{U}(t,t+dt)\right]$ above is a unitary operator written in the basis of the free-evolution hamiltonian, i.e. $\hat{H}_{atom}$. Expressed in terms of Pauli matrices, then

$$\hat{U}(t,t+dt) = \exp\left[-i\frac{\Omega_1(t)dt}{2}\hat{\sigma}_x\right]$$

where $\hat{\sigma}_x = |e\rangle\langle g| + |g\rangle\langle e|$. In the picture of a Bloch sphere, this corresponds to an infinitesimal rotation of the state vector by an angle $\frac{\Omega_1(t)}{2}dt$ with the x-axis being the axis of rotation. Therefore the cumulative effect of slowly fluctuating light's amplitude can be understood as being composed of a series of rotations around the x-axis, each time a different rotation angle ($d\theta = \Omega(t)dt$).

$$\begin{aligned} \hat{U}(0,T) &= \hat{U}(0,dt)\hat{U}(dt,2dt)...\hat{U}(t,t+dt)...\hat{U}(T-dt,T) \\ &= \exp\left[-\frac{i}{2}\underbrace{\left(\int_0^T \Omega_1(t')dt'\right)}_{\Theta}\hat{\sigma}_x\right] \end{aligned}$$

A π pulse therefore corresponds to $\Theta = \pi$ in this example.

A.2 Spontaneous Emission in Free Space

Consider a two-level system in the excited state at $t = 0$ as shown in Fig. A.2. The result derived in example 2 of the previous section predicts that the system will stay in the excited state forever if there is no external light to perturb this equilibrium. However, this is not true in reality where the excited state is actually observed to decay to the ground state even if there is no external light to interact

with. To explain such observations, one needs to take into account the interaction between the two-level system with all the vacuum radiation modes. This calls for a full quantum treatment of both the two-level system and the radiation modes. The following discussion follows the treatment of Weisskopf and Wigner [24].

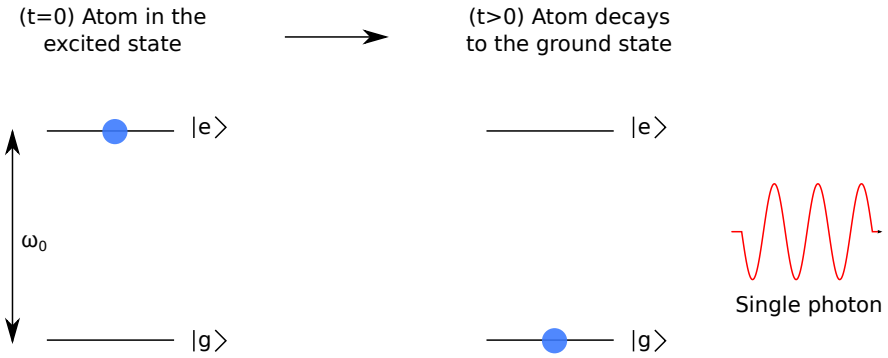

Figure A.2: Atom initially prepared in the excited state decays to the ground state through spontaneous emission emitting a single photon.

The electron - electromagnetic field interaction is assumed to be mainly dominated by the electric dipolar interaction. The total hamiltonian of the atom-light system under the rotating wave approximation is

$$\hat{H} = \hat{H}_{atom} + \hat{H}_{field} + \hat{H}_{dip} \tag{A.5}$$

, with

$$\begin{aligned}
\hat{H}_{atom} &= \hbar\omega_0 |e\rangle\langle e| \otimes \mathbb{1}_{field} \\
\hat{H}_{field} &= \mathbb{1}_{atom} \otimes \sum_{\{\vec{k},s\}} \hbar\omega_k (\hat{a}^\dagger \hat{a})_{\{\vec{k},s\}} \\
\hat{H}_{dip} &= -\hat{\vec{d}} \cdot \hat{\vec{E}} = \sum_{\{\vec{k},s\}} \hbar g_{\{\vec{k},s\}} |e\rangle\langle g| \otimes \hat{a}_{\{\vec{k},s\}} + h.c
\end{aligned}$$

In free space, we can consider a quantization cubic box of volume V with a periodic boundary condition. For such boundary condition, each radiation mode can be characterized by a wavevector $\vec{k}$ and the polarization $s = \{1, 2\}$. $\hat{a}_{\{\vec{k},s\}}$ and $\hat{a}^\dagger_{\{\vec{k},s\}}$ denote the annihilation and creation operator of the radiation mode

$\{\vec{k}, s\}$. The coupling factor $g_{\{\vec{k},s\}}$ is defined as

$$g_{\{\vec{k},s\}} = -\sqrt{\frac{\omega_k}{2\epsilon_0 \hbar V}} \vec{d}_{ge} \cdot \vec{\epsilon}_{\{\vec{k},s\}}$$

Expressed in the basis of the uncoupled atom-field system, the initial state can be written as $|\psi(0)\rangle = |e, \{0\}\rangle$ where $|\{0\}\rangle$ denotes that all the radiation modes are in vacuum state. From the form of the interaction hamiltonian, the state of the atom-field system at any later time can be expressed as

$$|\psi(t)\rangle = c_e(t)e^{-i\omega_0 t}|e, \{0\}\rangle + \sum_{\vec{k},s} c_{\{\vec{k},s\}}(t)e^{-i\omega_k t}|g, 1_{\{\vec{k},s\}}\rangle \tag{A.6}$$

where the state $|1_{\{\vec{k},s\}}\rangle$ denotes the radiation mode $\{\vec{k}, s\}$ having one photon and the rest are in vacuum mode. By solving the Schrödinger equation using the state decomposition in (A.6) and the hamiltonian in (A.5), this results in two coupled differential equations.

$$i\hbar \frac{d|\psi(t)\rangle}{dt} = \hat{H}|\psi(t)\rangle \rightarrow \left\{ \begin{array}{ll} \dfrac{dc_e(t)}{dt} & = -i \sum_{\{\vec{k},s\}} g_{\{\vec{k},s\}} c_{\{\vec{k},s\}}(t) e^{-i(\omega_k - \omega_0)t} \\ \dfrac{dc_{\{\vec{k},s\}}(t)}{dt} & = -i g^*_{\{\vec{k},s\}} c_e(t) e^{i(\omega_k - \omega_0)t} \end{array} \right\}$$

From the second equation, the coefficient $c_{\{\vec{k},s\}}(t)$ can be expressed in integral form and can be in turn used to solve for $c_e(t)$. This results in

$$\frac{dc_e(t)}{dt} = -\sum_{\{\vec{k},s\}} |g_{\{\vec{k},s\}}|^2 \int_0^t dt' c_e(t') e^{-i(\omega_k - \omega_0)(t-t')} \tag{A.7}$$

To solve this integro-differential equation, one can make several approximations. First of all, the amplitude $c_e(t)$ is assumed to vary slowly compared to the exponential term. For $t' < t$, the exponential term that oscillates rapidly is negligible except when $t' = t$. As such, we can approximate the value of $c_e(t')$ as a constant and replace it by its value at time t, i.e. $c_e(t)$. Since there is also little

contribution from $t' > t$, one can extend the integration limit to infinity. Denote $\tau = t - t'$, then

$$\begin{aligned}\int_0^t e^{-i(\omega_k-\omega_0)(t-t')}c_e(t')dt' &\approx c_e(t)\int_0^\infty d\tau e^{-i(\omega_k-\omega_0)\tau} \\ &= c_e(t)\pi\delta(\omega_k-\omega_0)\end{aligned}$$

For the summation over the modes $\{\vec{k}, s\}$ in (A.7), we can extend the volume of the quantization box to infinity. In this limit, the spacing between modes becomes smaller and the summation can be replaced by an integral.

$$\sum_{\{\vec{k},s\}} |g_{\{\vec{k},s\}}|^2 \xrightarrow[V\to\infty]{} \int \frac{V}{(2\pi)^3} d\vec{k} \sum_s \frac{\omega_k}{2\epsilon_0\hbar V} |\vec{d}_{ge}\cdot\vec{\epsilon}_{\{\vec{k},s\}}|^2$$

Denote the angle between the $\vec{k}$ and $\vec{d}_{ge}$ as θ. In free space, the wavevector $\vec{k}$ and the two orthogonal polarization vectors $\vec{\epsilon}_{\{\vec{k},1\}}$, $\vec{\epsilon}_{\{\vec{k},2\}}$ form an orthogonal basis from which any vector, including the electric dipole moment $\vec{d}_{ge}$ can be expanded. Therefore

$$\sum_{s=1,2} |\vec{d}_{ge}\cdot\vec{\epsilon}_{\{\vec{k},s\}}|^2 = |\vec{d}_{ge}|^2(1-\cos^2\theta) = |\vec{d}_{ge}|^2\sin^2\theta$$

Combining these results and recalling the dispersion relation $\omega_k = ck$, (A.7) becomes

$$\begin{aligned}\frac{dc_e(t)}{dt} &= -\left(\sum_{\{\vec{k},s\}} |g_{\{\vec{k},s\}}|^2\right) \times \left(\int_0^t dt' c_e(t') e^{-i(\omega_k-\omega_0)(t-t')}\right) \\ &= -\left(\int \frac{1}{(2\pi)^3} d\vec{k} \frac{\omega_k}{2\epsilon_0\hbar} |\vec{d}_{ge}|^2 \sin^2\theta\right) \times \pi\delta(\omega_k-\omega_0)c_e(t) \\ &= -\left(\frac{|\vec{d}_{ge}|^2}{(2\pi)^2 2\epsilon_0\hbar}\int_0^\infty k^2 dk \int_0^{2\pi} \sin^3\theta d\theta\right) \times \pi\delta(\omega_k-\omega_0)c_e(t) \\ &= -\frac{\omega_0^3|\vec{d}_{ge}|^2}{3\pi\epsilon_0\hbar c^3}\frac{c_e(t)}{2} \\ \frac{dc_e(t)}{dt} &= -\frac{\Gamma}{2}c_e(t)\end{aligned}$$

The constant Γ

$$\boxed{\Gamma = \frac{\omega_0^3 |\vec{d}_{ge}|^2}{3\pi\epsilon_0 \hbar c^3}}$$

is called the spontaneous decay rate and is defined such that the probability of the atom being in the excited state, i.e. $P_e(t) = |c_e(t)|^2$, decays exponentially at the rate of Γ.

$$\begin{aligned} \frac{dP_e(t)}{dt} &= -\Gamma P_e(t) \\ P_e(t) &= P_e(0)e^{-\Gamma t} \end{aligned}$$

Therefore a two-level atom initially prepared in the excited state will eventually decay to the ground state due to the interaction with the vacuum radiation modes. The decay can be characterized by the lifetime Γ which depends on the dipole matrix element between the ground and the excited state ($|\vec{d}_{ge}|$) and also the resonant frequency of the optical transition (ω_0). This decay would give rise to the emission of a single photon with the probability being in mode $\{\vec{k}, s\}$ is equal to $|c_{\{\vec{k},s\}}|^2$. This phenomenon of the excited atom emitting a single photon in the absence of external light is referred to as the spontaneous emission.

References

[1] Gisin, N. & Thew, R. Quantum Communication. *Nature Photonics* 165–171 (2007). URL http://www.nature.com/nphoton/journal/v1/n3/abs/nphoton.2007.22.html. 1

[2] Kok, P., Nemoto, K., Ralph, T. C., Dowling, J. P. & Milburn, G. J. Linear optical quantum computing with photonic qubits. *Reviews of Modern Physics* **79**, 135–174 (2007). URL http://link.aps.org/doi/10.1103/RevModPhys.79.135. 1

[3] Kimble, H. J. The Quantum Internet. *Nature* **453**, 1023–30 (2008). URL http://www.ncbi.nlm.nih.gov/pubmed/18563153. 1

[4] Wineland, D. J. *et al.* Quantum information processing with trapped ions. *Philosophical transactions. Series A, Mathematical, physical, and engineering sciences* **361**, 1349–61 (2003). URL http://www.ncbi.nlm.nih.gov/pubmed/12869312. 1

[5] Jessen, P. & Stock, R. Quantum information processing with trapped neutral atoms. *Quantum Information Processing* **3**, 91–103 (2004). URL http://link.springer.com/article/10.1007/s11128-004-9418-2. 1

[6] Enk, S. V., Kimble, H. & Mabuchi, H. Quantum information processing in cavity-QED. *Experimental Aspects of Quantum ...* **3**, 75–90 (2005). URL http://link.springer.com/chapter/10.1007/0-387-27732-3_6. 1

[7] Wrachtrup, J. & Jelezko, F. Processing quantum information in diamond. *Journal of Physics: Condensed Matter* **18**, S807–S824

(2006). URL http://stacks.iop.org/0953-8984/18/i=21/a=S08?key=crossref.3ebf978682f06b8bfab48217febea4e1. 1

[8] Tey, M. K. *et al.* Strong interaction between light and a single trapped atom without the need foracavity. *Nature Physics* **4**, 924–927 (2008). URL http://www.nature.com/doifinder/10.1038/nphys1096. 1, 3, 5, 7, 12

[9] Srivathsan, B. *et al.* Narrow Band Source of Transform-Limited Photon Pairs via Four-Wave Mixing in a Cold Atomic Ensemble. *Physical Review Letters* **111**, 123602 (2013). URL http://link.aps.org/doi/10.1103/PhysRevLett.111.123602. 2, 34

[10] Hong, C., Ou, Z. & Mandel, L. Measurement of subpicosecond time intervals between two photons by interference. *Physical Review Letters* (1987). URL http://www.inoa.it/home/azavatta/References/PRL59p2044.pdf. 2

[11] Metcalf, H. & van der Straten, P. *Laser cooling and trapping* (Springer Science, 1999). 3, 32

[12] Schlosser, N., Reymond, G. & Grangier, P. Collisional Blockade in Microscopic Optical Dipole Traps. *Physical Review Letters* **89**, 023005 (2002). URL http://link.aps.org/doi/10.1103/PhysRevLett.89.023005. 4

[13] Schlosser, N., Reymond, G., Protsenko, I. & Grangier, P. Sub-poissonian loading of single atoms in a microscopic dipole trap. *Nature* **411**, 1024–7 (2001). URL http://www.ncbi.nlm.nih.gov/pubmed/11429597. 4

[14] Tey, M. K. *et al.* Interfacing light and single atoms with a lens. *New Journal of Physics* **11**, 043011 (2009). URL http://stacks.iop.org/1367-2630/11/i=4/a=043011?key=crossref.e4161d364d25c1611ff4b3faaba72b5a. 14

[15] Volz, U. & Schmoranzer, H. Precision lifetime measurements on alkali atoms and on helium by beamgaslaser spectroscopy. *Physica Scripta* **48** (1996). URL http://iopscience.iop.org/1402-4896/1996/T65/007. 27

[16] Rotberg, E. a. *et al.* Measurement of excited-state lifetime using two-pulse photon echoes in rubidium vapor. *Journal of the Optical Society of America B* **24**, 671 (2007). URL http://www.opticsinfobase.org/abstract.cfm?URI=josab-24-3-671. 27

[17] Feichtner, J., Gallagher, J. & Mizushima, M. Lifetime of the First Excited Atomic States of Rb87. *Physical Review* **164** (1967). URL http://prola.aps.org/abstract/PR/v164/i1/p44_1. 28

[18] Darquié, B. *et al.* Controlled single-photon emission from a single trapped two-level atom. *Science (New York, N.Y.)* **309**, 454–6 (2005). URL http://www.ncbi.nlm.nih.gov/pubmed/16020731. 31

[19] Malinovsky, V. & Krause, J. General theory of population transfer by adiabatic rapid passage with intense , chirped laser pulses. *The European Physical Journal D* **155**, 147–155 (2001). URL http://link.springer.com/article/10.1007/s100530170212. 32

[20] Abragam, A. *The Principles of Nuclear Magnetism* (Oxford University Press, 1961). 32

[21] Loy, M. Observation of Population Inversion by Optical Adiabatic Rapid Passage. *Physical Review Letters* **32**, 814–817 (1974). URL http://prl.aps.org/abstract/PRL/v32/i15/p814_1. 32

[22] Cohen-Tannoudji, C., Dupont-Roc, J. & Grynberg, G. *Atom-Photon Interactions: Basic Processes and Applications* (WILEY-VCH, 2004). 35

[23] Steck, D. A. *Quantum and Atom Optics* (2013), (revision 0.9.8, 12 september 2013) edn. URL http://steck.us/teaching. 35

[24] Weisskopf, V. & Wigner, E. Berechnung der natürlichen linienbreite auf grund der diracschen lichttheorie. *Zeitschrift für Physik* 54–73 (1930). URL http://link.springer.com/article/10.1007/BF01336768. 40